Damage mechanisms of ultrahigh strength steels in bending application to a trip steel

Delphine Reche, T. Sturel, Anne-Françoise Gourgues-Lorenzon, Jacques Besson

DAMAGE MECHANISMS OF ULTRAHIGH STRENGTH STEELS IN BENDING APPLICATION TO A TRIP STEEL

D. Rèche [1), 2)], T. Sturel [2)], A.F. Gourgues-Lorenzon [1)], J. Besson [1)]

[1)] MINES ParisTech, Centre des Matériaux, CNRS UMR 7633, BP 87
91003 Evry Cedex, France
[2)] ArcelorMittal Global R&D, Voie Romaine, BP 30320,
57283 Maizières-lès-Metz Cedex, France

ABSTRACT

In order to optimize their metallurgical quality, the present study aims at understanding damage mechanisms involved in bending of Ultra High Strength Steels (UHSSs). It focuses on a TRansformation Induced Plasticity (TRIP)-aided steel.
This work is based on three complementary approaches: first, instrumented V-bending and stretch bending tests that are usually performed to compare the bending behaviour of various steels, then, metallographic observations carried out to investigate damage initiation and finally, simulation of bending tests by finite element methods.
Three-point-bending and stretch bending tests involve different crack initiation areas. Metallographic observations performed on V-bent specimens show crack initiation just below the outer surface, whereas in a stretch bending test, the crack clearly initiates from the central segregation (if any).
V-bending tests were modelled with a finite element simulation approach to assess the stress and strain fields by comparison with experimental results. Modelling of stretch bending is currently in progress.

KEYWORDS

Ultrahigh strength steels, TRIP steels, V-bending, stretch bending, microstructure, fracture mechanisms

INTRODUCTION

Advanced high strength steels are more and more intensively used in the automotive industry for weight and cost reduction as well as for crash performance improvement. As these steels are used to make safety and structural parts such as bumper reinforcements and intrusion beams, they have to combine a relatively good formability with high strength.
Figure 1 shows the relationship between tensile strength and fracture elongation of several classes of steel sheets available to the automotive industry.

Good elongation and high strength can be obtained by the combination of several phases (DP, TRIP steels for instance). However, a drop of formability is sometimes experienced under severe conditions, in particular forming modes such as bending. To promote the use of these steels, it is therefore essential to get a better understanding of the links between microstructure and failure mechanisms during bending in order to improve their bending ability. This is the aim of this study, which concentrates on a TRIP steel sheet.

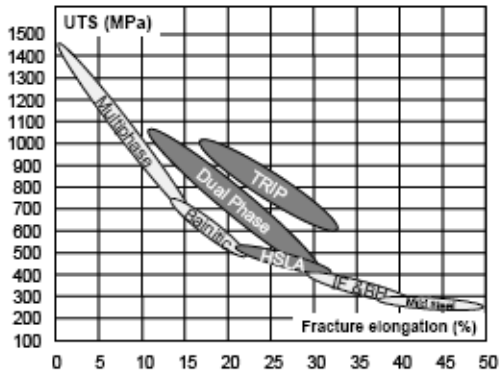

Fig. 1: Ultimate tensile strength and fracture elongation for main steel product families [1]

The formability of sheet metals often refers to the limit of strain or stress states up to which the forming process is accomplished successfully without failure. However, Yamazaki *et al.* [2] showed that the formability of UHSSs (with a tensile strength higher than 780 MPa) correlates with bending ability better than with total elongation in tensile tests. This means that the formability of UHSSs is governed by local ductility that can be evaluated by bending ability.
Steninger *et al.* [3] performed V-bending tests on steels with tensile strength between 240 and 390 MPa and a thickness of 5 mm. They observed cracks on outer surfaces of the specimens. Fracture propagated along shear bands and voids expanded preferentially along the shear direction.

In the automotive industry, many such parts are stamped, so a laboratory test that represents stamping better than the V-bending test is needed. The stretch bending test (fig. 4), which combines bending and tensile loading, seemed to be the closest bending test to represent stamping. The stretch bending ability is often represented by the punch displacement at failure as a function of the (R/t) ratio, R being the punch radius and t the sheet thickness. It was shown that, above a critical value of the (R/t) ratio, failure moved from the punch nose to the sidewall because stretching becomes predominant over bending [4, 5, 6].

The present paper is an in-depth investigation of damage modes and fracture mechanisms in both V-bending and stretch bending conditions. The study is organized in 3 parallel tasks: global characterization of the studied materials, fine observations of damage by metallographic examinations and numerical simulation of the tests in order to confirm or invalidate hypotheses about failure mechanisms.

SPECIMENS, MATERIAL AND TESTING

Material

The study focuses on a TRIP steel (C~0.2 wt%, Mn~1.6 wt%) of 1.6 mm in thickness whose mechanical properties are reported in table 1.
Its microstructure consists of hard martensite/austenite islands in a softer ferritic matrix (figure 2). In order to study the possible influence of central segregation, processing conditions were chosen to enhance segregation in this sheet. The third-thickness microstructure is rather homogeneous with austenite and martensite islands within ferrite, while on the mid-thickness microstructure, we can distinguish a central segregation surely due to segregation of austenite forming elements. Hard phases are present as 2-5 µm islands linked by fine bands of smaller islands.

Fig. 2: Light optical micrographs of the TRIP steel along rolling direction, LePera etching. Left: third-thickness microstructure, right: mid-thickness microstructure. Hard phases (austenite + martensite) in white, ferrite in brown.

Dir.	YS (MPa)	TS (MPa)	Uniform El. (%)	Total El. (%)
RD	467	866	15.0	20.0
TD	546	851	15.0	19.2

Table 1: Room temperature mechanical properties along rolling (RD) and transverse (TD) directions (Sample 20x80mm ISO)

Testing

To investigate the bending ability of this steel, two tests were used: a simple 3-point-bending test (fig. 3) and a stretch-bending test (fig. 4), both at room temperature.

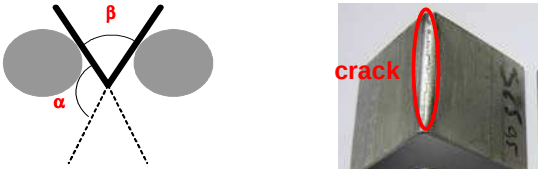

Fig. 3: V-bending test. Left: schematics; right: V-bending specimen after cracking

The V-bending test was carried out on a universal tensile machine, with two rotary rolls and various punches available (bending radius from 0 to 15 mm). The edges of the samples (size: 100 mm in length and 50 mm in width) were ground before testing to avoid cracks starting from edges. Five samples per direction (rolling and transverse directions) were bent with a punch radius close to 0 mm.
The test was stopped when the first crack appeared. Then, the bending angle (β in figure 3) was measured after specimen unloading thanks to a protractor. This test is generally used to compare the bending ability of various steels.

The method for stretch bending tests consists in clamping specimens between a die and a blank holder. Here also, the edges of the samples (250 mm in length and 40 mm in width) were ground before testing to avoid cracks starting from edges and five samples were bent per direction.

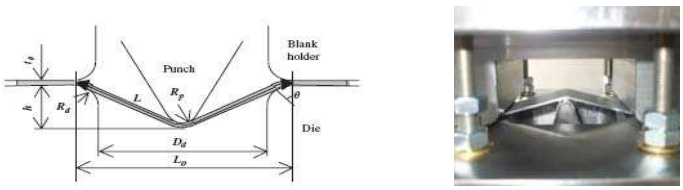

Fig. 4: Stretch bending test. Left: schematics; right: test in progress

This test makes it possible to determine punch displacement at failure for various punch radii, and therefore enables to rank material formability for different R/t ratios.

For the two tests (V-bending and stretch bending), the reproducibility was good and a cracking anisotropy was observed. Specimens taken along the rolling direction showed better ability in bending than specimens taken along the transverse direction.

EXPERIMENTAL RESULTS

Coupling of forming tests and metallurgical observations aims at determining the most influent metallurgical parameters acting on bending or stretch-bending performance (role of the banded structure, the central segregation, the phase distribution, etc.).

V-bending

In V-bending (fig. 5), cracks seem to initiate from the outer surface or, as suggested by the V shape of some of the micro cracks (figure 5, rights), just below the outer surface. In this last case, this could result from the most detrimental combination of locally high tensile stress and lower local damage resistance linked to a banded structure. Nevertheless, from these first observations, it is not possible to fully conclude on this point. The only similar feature is the angle of about 45° with the outer surface for the two cracks. This confirms the shear mode crack propagation already observed by Steninger *et al*. [2].

Moreover, on one sample with a very small crack and a locally very thick segregation band, damage was observed in the central segregation area (dark dots in figure 6), and also what appears to be local necking. This suggests that the central segregation area is probably not located at the neutral fibre during the entire test but in the tensile zone (fig. 6). Nevertheless, this damage mechanism does not seem to have influenced cracking for this kind of test.

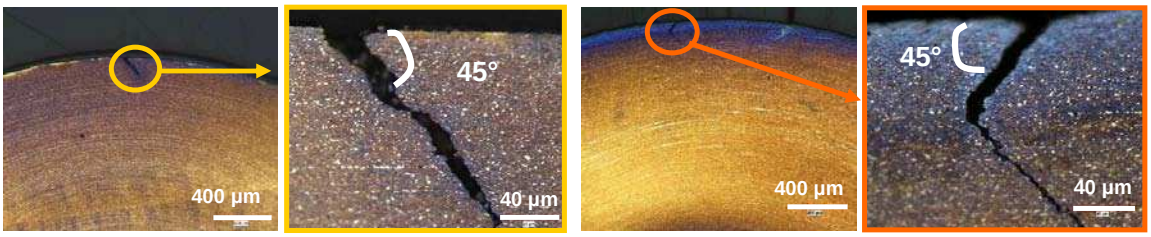

Fig. 5: V-bending specimens. Optical micrographs, LePera etching

Fig. 6: Local necking around the central segregation band, optical micrographs, LePera etching

Stretch bending

In stretch-bending, cracking clearly initiates from the central segregation area. This was demonstrated, despite the high mechanical instability of failure during this test, by some longitudinal cross-section observations of internal arrested cracks (fig. 7, 8).

Fig. 7: Broken stretch bent specimen and damage at the central segregation area. Optical micrographs, LePera etching

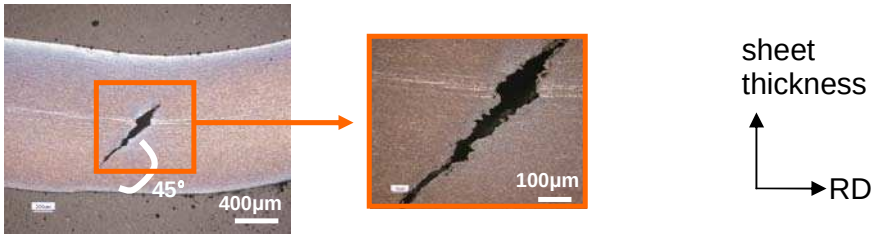

Fig. 8: Stretch bent specimen; the test was interrupted after internal cracking. Optical micrographs, LePera etching

MECHANICAL ANALYSIS OF THE TESTS

In order to get a better understanding of these results, numerical simulations of these tests were carried out. The main aims for this study are to assess the stress and strain fields for V-bending and stretch bending tests and to investigate a fracture criterion for these tests.
In this part of the study, the steel was considered as a homogeneous material. Neither the phase transformation of retained austenite into martensite nor the presence of segregation bands were explicitly taken into account.

The in-house finite element software Z-set [7] was used to simulate all mechanical tests. An implicit scheme was used to integrate constitutive equations. All calculations were done using linear elements with full selective integration and updated Lagrangian formulation.
Material constitutive equations included both isotropic and kinematic hardening. The steel sheets being anisotropic, an anisotropic yield criterion was used. Isotropic hardening and yield anisotropy parameters were fitted thanks to tensile tests on smooth and notched specimens. Shearing tests were performed to investigate the kinematic part of hardening.
Two anisotropic yield criteria were tested: Barlat 91 model [8] and the Bron Besson one [9]. A better fit was obtained with the Bron Besson model, so this is the chosen model. It included two non-linear kinematic hardening variables (four fitting parameters), one non-linear isotropic variable (two fitting parameters) and some linear isotropic hardening (one fitting parameter, mandatory for large strains experienced during tension of notched specimens and during bending). The model together with the fitted parameters well reproduced tensile curves, reverse shearing curves (up to 30% strain) as well as Lankford anisotropy coefficients (smooth tensile tests) [10] (fig. 9).

Only results concerning the V-bending test are presented here. The simulation of stretch bending is still in progress.

Modelling of the V-bending test

The simulation has mainly been performed in plane strain (2D) conditions. The tools (punch + roll) were simulated with an elastic behaviour (E = 210 GPa) and the sheet with the above determined constitutive equations.

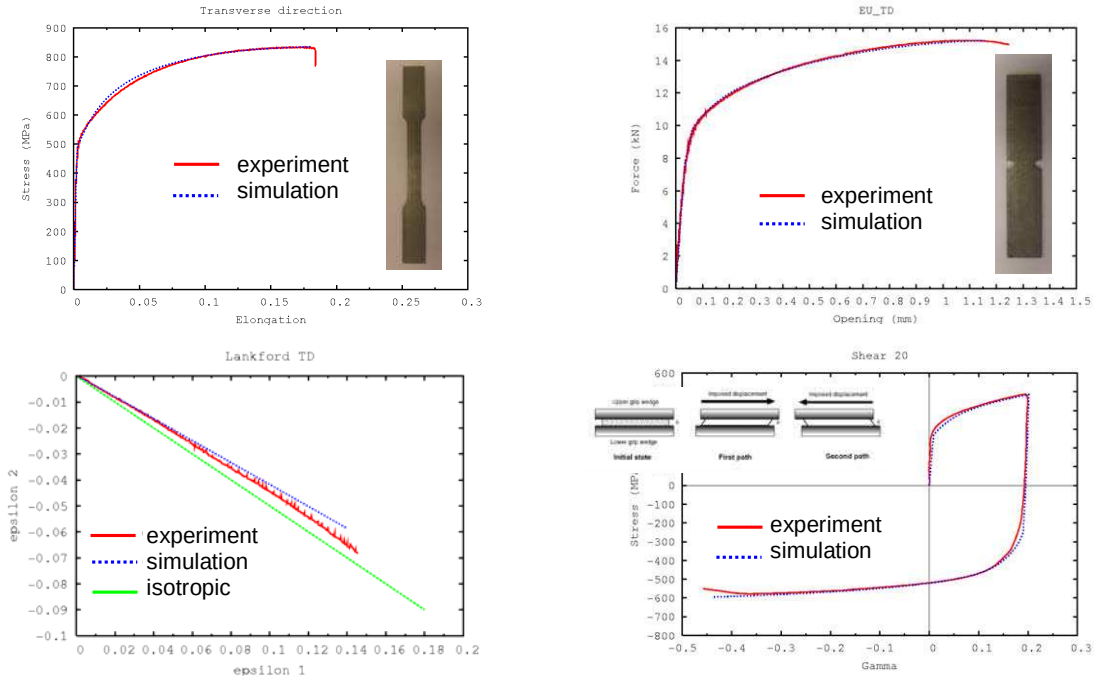

Fig. 9: Tensile curves (smooth and notched samples), Lankford curves and shearing curves along the transverse direction (experiment vs. model predictions)

For this test, two contact conditions were modelled: first, the sheet with the punch, where the friction coefficient is equal to 0.25, then, the contact between the sheet and the roll, where the friction coefficient of the Coulomb law is equal to 0. In fact, during the test, rolls turn with the sample so the hypothesis that there is no significant friction between the sample and the roll was made. Here, calculations were performed with 32 elements in the thickness. Similar results were found if replacing the punch by prescribed displacement of the nodes along the symmetry plane.
The mesh of this test is represented in figure 10 with only one half of the specimen and punch and one roll because of the symmetry conditions. As very little deformation occurs along the specimen width, plane strain conditions were first assumed to make two-dimensional calculations.

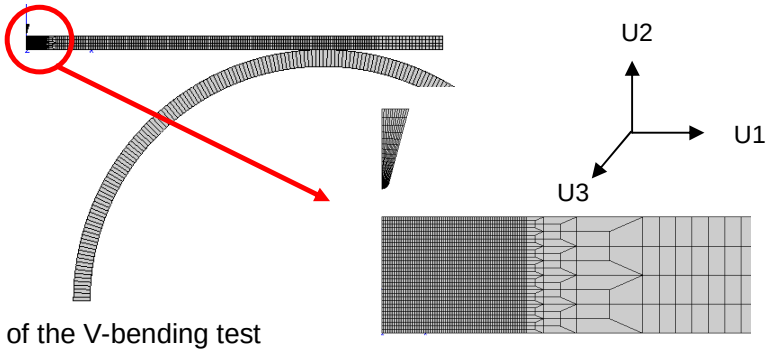

Fig. 10: Meshing of the V-bending test

Figure 11 reports load/displacement curves obtained respectively with the V-bending test (experiment) and the numerical simulation. At the beginning of the test, the elastic part is seen (punch displacement up to about 2 mm). Then the plastic part of the test is observed and the load increasing up to a maximum. After a load drop by about 5%, the test is stopped because of the onset of cracking at the bend nose. Good agreement concerning the prediction of the curve can be noticed. However, the simulated curve somewhat departs from

the experimental curve just after the elastic part with a simulated load lower than the experimental one. At the end of the test, the tendency is reversed.

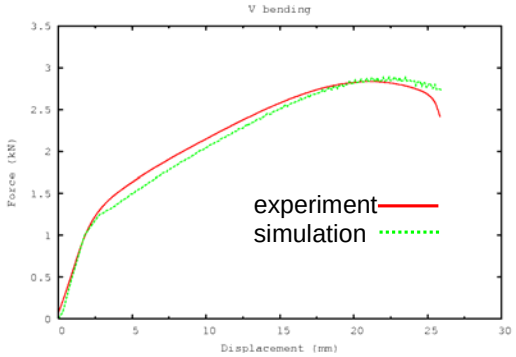

Fig. 11: V-bending test: experimental load-displacement curve vs. simulation predictions

The stress and strain fields at the end of the test are shown in figure 12. It is noticed that the neutral fibre (σ_{11} = 0 and ε_{11}=0) is not at mid-thickness. Thus, numerical simulations confirm that the mid-thickness area is in the tensile zone as suggested by previous damage observations (fig. 6).

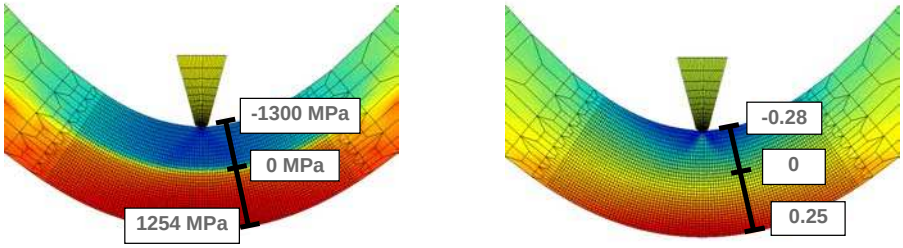

Fig.12: Stress and strain fields for a punch displacement of 26mm, punch radius 0.1 mm, Left:σ_{11} map , right: ε_{11} map

In order to check the plane strain hypothesis of the 2D simulation, calculations were also carried out in three dimensions by meshing 16 elements in the thickness and 5 in the width. One reference calculation was also performed with 32 elements in the thickness and similar results were found, so that 16 elements were used for the rest of calculations. The punch was replaced by prescribed displacement boundary conditions and modelling was performed with ¼ of the sample and half a roll due to the symmetry conditions.
Figure 13 shows load / displacement curves obtained both with 2D and 3D simulations. The two curves are similar, which shows that plane strain 2D simulation can be used for modelling this test in the considered geometric conditions.

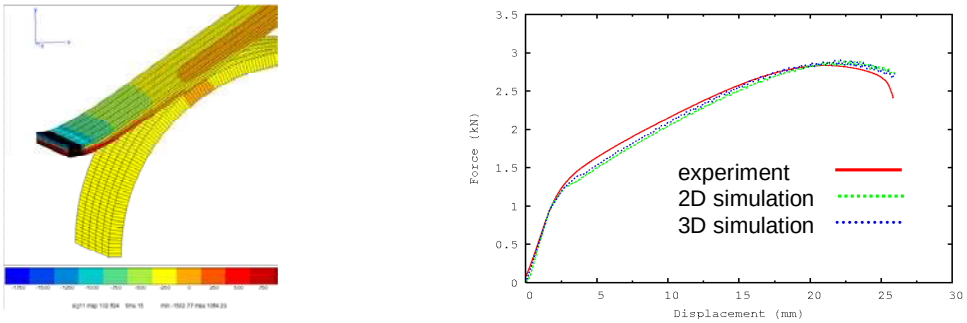

Fig. 13: Left: σ_{11} map of the 3D V-bending test ($\sigma_{11\ max}$=1084 MPa, $\sigma_{11\ min}$=-1562 MPa), punch displacement of 26 mm, right: Experimental load/displacement curve vs. curves predicted using 2D and 3D calculations.

SUMMARY AND CONCLUSIONS

Crack initiation mechanisms differ between the V-bending and the stretch bending tests. In V-bending specimens, cracks seem to initiate from the surface or just below while in stretch bending, cracks initiate from the central segregation. Moreover, in V-bending, necking was observed at the central segregation together with cavities (damage), which confirms that the central segregation area is, in fact, slightly loaded in tension. This was confirmed by numerical simulation.
To model V-bending and stretch bending tests thanks to finite element numerical simulation, constitutive equations of the steel were determined and parameters fitted using tensile tests on smooth and notched samples and shearing tests. The Bron Besson model with isotropic and kinematic hardening rules was adopted. The V-bending test was then simulated, which yielded good results in terms of load/displacement curve with no fracture criterion in the model. Moreover, 3D simulations confirmed the validity of the choice of the plane strain hypothesis.
Now, it is necessary to perform numerical simulation of the stretch bending test and to introduce a fracture criterion in the model in order to better fit experimental observations.

REFERENCES

[1] Bretault, N.:
Développement des aciers THR pour application automobile
Séminaire du Centre des Matériaux de l' Ecole des Mines de Paris (avril 2007)
[2] Yamazaki, K.; Oka, M.; Yasuda, H.; Mizuyama, Y.; Tsuchiya, H.:
Recent Advances in UHSS for automotive structural use
Nippon steel technical report (1995) No. 64
[3] Steninger, J.; Melander, A.:
The relation between bendability, tensile properties and particle structure of low-carbon steel
Scandinavian Journal of Metallurgy 11 (1982) No. 2, pp. 55-71
[4] Demeri, M.Y.:
The stretch bend forming of sheet metal
Journal of Applied Metalworking 2 (1981), pp. 3-10
[5] Sadagopan, S.; Wong, C.; Huang, M.; Yan, B.:
Stretch bendability of advanced high strength steels
SAE International (2003), pp.107-115
[6] Hudgins, A.; Matlock, D.; Speer, J.; Fekete, J.; Walp, M.:
The susceptibility to shear fracture in bending of advanced high strength sheet steels
MS&T Conference Proceedings, Detroit, (2007), pp. 145-157
[7] Besson, J.; Foerch, R.:
Large scale object-oriented finite element code design
Comp Meth Appl Mech Engng 87 (1997), pp. 142-165
[8] Barlat, F.; Lege, D.J.; Brem, J.C.:
A six component yield function for anisotropic materials
International Journal of Plasticity 7 (1991), pp. 693-712
[9] Bron, F.; Besson, J.:
A yield function for anisotropic materials. Application to aluminium alloys
International Journal of Plasticity 20 (2004), pp. 937-963
[10] Rèche, D.:
Relations between microstructure and formability on UHSS for automotive products
Ph.D thesis in progress (2008-2011)

Corresponding author: delphine.reche@ensmp.fr